International Journal of Nanomedicine

Dovepress
open access to scientific and medical research

Open Access Full Text Article

ORIGINAL RESEARCH

ROS-Responsive Chitosan Coated Magnetic Iron Oxide Nanoparticles as Potential Vehicles for Targeted Drug Delivery in Cancer Therapy

This article was published in the following Dove Press journal:
International Journal of Nanomedicine

Srinivasan Ayyanaar[1]
Chandrasekar Balachandran[2]
Rangaswamy Chinnabba Bhaskar[3]
Mookkandi Palsamy Kesavan[4]
Shin Aoki[2,5]
Ramachandran Palpandi Raja[6]
Jegathalaprathaban Rajesh[7]
Thomas J Webster[8]
Gurusamy Rajagopal[1]

[1]PG and Research Department of Chemistry, Chikkanna Government Arts College, Tiruppur 641 602, Tamilnadu, India; [2]Faculty of Pharmaceutical Sciences, Tokyo University of Science, Noda 278-8510, Japan; [3]Department of Chemistry, School of Advanced Sciences, Vellore Institute of Technology, Vellore 632014, Tamil Nadu, India; [4]Department of Chemistry, Hajee Karutha Rowther Howdia College, Uthamapalayam 625 533, Tamil Nadu, India; [5]Research Institute of Science and Technology, Tokyo University of Science, Noda 278-8510, Japan; [6]Centre for Biotechnology, Anna University, Chennai 600 025, Tamil Nadu, India; [7]Chemistry Research Centre, Mohamed Sathak Engineering College, Kilakarai 623 806, Tamil Nadu, India; [8]Department of Chemical Engineering, Northeastern University, Boston, MA 02115, USA

Correspondence: Jegathalaprathaban Rajesh; Thomas J Webster
Email mkuraji@gmail.com; th.webster@neu.edu

Background and Objective: Cancer cells accumulate high concentrations of reactive oxygen species as a result of their faster and uninhibited metabolic activity. Cancer chemotherapeutic agents release an excess of severe adverse reactions as a result of targeting normal cells. This demands an improvement in targeted drug-delivery systems to selectively discharge anticancer drugs in the vicinity of such highly metabolically and mitotically active cells.

Materials and Methods: Here, magnetic nanoparticles were synthesized by a traditional co-precipitation technique. Fe_3O_4@OA-CS-5-FLU-NPs were synthesized by an easy and rapid in situ loading method. The proposed Fe_3O_4@OA-CS-5-FLU-NPs were productively prepared as well as characterized by various spectroscopic and microscopic studies.

Results: The targeted drug release profile of the Fe_3O_4@OA-CS-5-FLU-NPs was studied in the presence of ROS including H_2O_2 and pH induction. The released product, Fe_3O_4@OA-CS-5-FLU-NP, exhibited desirable levels of cytotoxicity and demonstrated morphological changes and inhibition of colony formation for A549 and HeLa S3 cancer cells. The IC50 values at 24 hours were 12.9 and 23 μg/mL, respectively.

Conclusion: In summary, results from the MTT assay, fluorescence staining as well as colony formation assays, revealed that the Fe_3O_4@OA-CS-5-FLU-NPs were active and safe for anticancer biomedical applications. In summary, the present investigation provides a powerful nanostructured based system for improved cancer theranostics that should be further studied.

Keywords: magnetic iron oxide nanoparticles, oleic acid, chitosan, 5-fluorouracil, cytotoxicity, targeted drug delivery

Introduction

Successful cancer therapy depends on the outcome of surgical resection of the affected tissue in combination with chemotherapy or radiation therapy.[1–3] Although anticancer drugs are efficient at destroying tumor cells, they are potentially harmful as a result of their non-selectivity, which has limited their therapeutic use.[4–6] In the last few decades, there have been more and more cases of nanoparticles (NPs), such as Fe_3O_4NP, which have played a pivotal role in drug delivery specifically targeting cancer cells.[7] Fe_3O_4NP have gained great attention in various biomedical applications such as targeted delivery, localized hyperthermia treatment, as well as contrast agents for magnetic resonance imaging (MRI).[8–10] As the Fe_3O_4NP are unstable in aqueous media, they cannot be used as drug carriers alone. In order to overcome this drawback, a coating is applied to employ lipids, proteins, carbohydrates, liposomes, synthetic and bio-degradable polymers.[11–14]

submit your manuscript | www.dovepress.com
DovePress
http://doi.org/10.2147/IJN.S249240

Chitosan has been proposed as a potential carrier for drugs and biological macromolecules[15] with potential biomedical and pharmacological applications because of several attractive features such as low cost, safety, biodegradability and biocompatibility.[16–18] Chitosan and its derivatives have many desirable biological and biochemical properties which could be attributed to reactive functional groups namely hydroxyl (-OH) and amino ($-NH_2$) groups. On the other hand, chitosan is not suitable for binding to Fe_3O_4NP as the resulting magnetic compounds tend to form aggregates of polymer cross-linked complexes and polymer adsorbates.[19,20]

Many investigators have attempted to functionalize CS in order to bind onto Fe_3O_4NP. Several reports highlight the internalization of some Fe_3O_4NP with an enhanced generation of reactive oxygen species (ROS). Enhanced ROS levels have demonstrated synergistic antitumor efficacy by stimulating mitochondria-meditated apoptosis.[21–24]

Fe_3O_4NP have been reported to up-regulate ROS including H_2O_2 which potentially play a key role in biomedical applications especially for targeted drug delivery.[25] The assessment of anticancer drug-loaded nanoparticles and their effect on the induction of cell apoptosis, and the extent of the Fe_3O_4NP activated ROS-mediated mitochondrial apoptosis pathway, have not been experimentally investigated. 5-FLU is an anti-metabolite of the pyrimidine class, with a broad spectrum of activity and is quite effective in the chemotherapy of solid malignant tumors, such as that of the abdominal cavity, ovary, liver, brain, breast, etc., either alone or in combination.[26,27] 5-FLU affects nucleoside uptake and can be incorporated into RNA as well as DNA, leading to cytotoxicity and cell damage. Oleic acid (OA) is a commonly used surfactant to stabilize magnetic nanoparticles synthesized by traditional co-precipitation methods, and some studies have proved that a strong chemical bond is formed between carboxylic acid and amorphous iron and amorphous iron oxide nanoparticles. OA possesses a non-polar hydrocarbon tail and a polar carboxylic acid head group. Carboxylate anions are known to coordinate with the surface of magnetite, presumably through a coordination of iron atoms with both of the carboxylate oxygens. Oleic acid and chitosan-based magnetic aggregates were investigated here as a controlled drug-delivery system capable of pH alteration and ROS release.[28,29] They also exhibit enhanced levels of biocompatibility as well as desirable drug release characteristics.[30]

Herein, we present the synthesis, characterization and evaluation of Fe_3O_4@OA-CS-5-FLU-NPs as a combination drug carrier for the pH-responsive release of 5-FLU delivery in A549 and HeLa S3 cell cultures and the resultant synergistic cytotoxicity of 5-FLU and ROS.

Materials and Methods

Chemicals

Iron (II) tetrahydrate ($FeCl_2{\cdot}4H_2O$), iron (III) chloride hexahydrate ($FeCl_3{\cdot}6H_2O$), sodium hydroxide and oleic acid (OA) were purchased from Merck (India). Chitosan (CS) and 5-fluorouracil (5-FLU) were procured from Sigma-Aldrich. Milli-Q water and organic solvents of analytical grade were used in this study.

Preparation of Fe_3O_4@OA NPs

Fe_3O_4 magnetic nanoparticles were synthesized by a chemical co-precipitation process. Concisely, 1.0 g of $FeCl_3{\cdot}6H_2O$ and 0.5 g of $FeCl_2{\cdot}4H_2O$ were dissolved in 50 mL of double-distilled water through a dynamic stirring process and the solution was allowed to reflux at 80 °C. Then, the precipitant of the ammonia solution in 10 mL (NH_4OH, 25 wt %) was slowly dropped into the above mixture under vigorous stirring for 15 min;[31] the reason for using an ammonia solution was to increase the number and size of the nanoparticles. Ammonia could play a role not only in increasing the reaction rate but also in retarding the growth of the particles when used in different concentration ranges. Finally, the drop-wise addition of oleic acid (3 mL) into the above suspension led to an alteration at the surface of the Fe_3O_4NP.[27] This mixture was refluxed at 80 °C for 30 min to complete the formation of the Fe_3O_4 NP. Subsequently, the suspension was cooled down to room temperature and separated by a magnet, cleaned with distilled water and ethanol to remove the reactants and impurities. The final product of Fe_3O_4@OA NP (oil-base surface) was desiccated at room temperature under a vacuum at 60 °C for 12 h.

Preparation of Fe_3O_4@OA-CS-NPs

Chitosan modified Fe_3O_4NPs were synthesized by the co-precipitation of Fe^{2+} and Fe^{3+} salts in the presence of chitosan.[32] Chitosan (0.125 g) was solidified in 30 mL of 1% acetic acid and the pH was tuned to 4.8 by adding 10 M NaOH. The Fe_3O_4@OA NPs (1g) were added to 30 mL of a chitosan solution while stirring under an inert atmosphere at 50 °C. Then, 30 mL of an aqueous ammonia solution (25%) was gently added to the above mixture to yield small nanoparticles. The resulting mixture was further stirred for

30 min. The colloidal Fe_3O_4@OA-CS-NP was continuously washed with distilled water and separated by magnetic decantation repeatedly.

Preparation of Fe_3O_4@OA-CS-5-FLU-NPs

Fe_3O_4@OA-CS-5-FLU-NPs were prepared based on an in situ filling process as shown in Figure 1. For the loading method, Fe_3O_4@OA-CS-NPs (100 mg) were mixed with 5-FLU and stirred at room temperature for 48 h. The negatively charged 5-FLU molecules electrostatically interacted with positively charged CS molecules for the formation of Fe_3O_4@OA-CS-5-FLU-NPs. Chitosan is a hydrophilic cationic polymer used to prepare nanoparticles by means of electrostatic interactions. 5-fluorouracil (5-FU) is a hydrophilic drug. Two ionic interactions exist in the reaction process: an intense electrostatic interaction between the positively charged amino group of CS and the negatively charged 5-FLU solution. The suspension was carefully collected using a magnet and washed with an abundant amount of water and ethanol to remove the unreacted particles. Finally, the Fe_3O_4@OA-CS-5-FLU-NP powder was obtained after drying under vacuum pressure.[33]

Characterization of Fe_3O_4 @OA-CS-5-FLU-NPs

Powder X-ray diffraction (XRD) of Fe_3O_4@OA-CS-5-FLU-NP was analyzed by a X'Perto Pro, PANalytical X-ray diffractometer using a CuKα energy source (λ=1.5406 Å). The Fe_3O_4@OA-CS-5-FLU-NPs were further characterized using a Perkin Elmer Fourier transform-infra red (FT-IR) spectrophotometer. Transmission electron microscopy (TEM) and scanning electron microscopy (SEM) micrographs of the Fe_3O_4@OA-CS-5-FLU-NP were collected using a JSM-6390LVJEOL (Japan) to analyze surface morphology. The magnetic properties of the Fe_3O_4@OA-CS-5-FLU-NPs were studied using a Lakeshore 7404-vibrating sample magnetometer (VSM) at room temperature. Thermogravimetric analysis (TGA) was done on a SDT Q600 (USA) TA instrument.

Estimation of Drug Encapsulation Efficiency of Fe_3O_4@OA-CS-5-FLU-NPs

The concentration of the Fe_3O_4@OA-CS-5-FLU-NP was estimated by UV-Vis spectrophotometry. 10 milligrams of Fe_3O_4@OA-CS-5-FLU-NP dissolved in 1 mL of DCM (dichloromethane, to allow for a more extensive and increased drug-loading into the interior of nanoparticle) was taken in a closed glass tube and 10 mL of phosphate buffer (pH 7.4) was added to it (the total volume of the releasing medium was maintained as constant by adding an equal volume of fresh buffer solution). The mixture was stirred for 2h at room temperature. The mixture was centrifuged at 6000 rpm for 10 min after the slow evaporation of DCM. The buffer solution was separated and the amount of 5-FLU in the buffer solution was estimated by spectrophotometry at 270 nm. The following equations were used to determine drug content and encapsulation efficiency:

$$\text{Drug content} = \frac{\text{Weight of encapsulated drug in nanoparticles}}{\text{Weight of nanoparticles}} \times 100$$

$$\text{Encapsulation efficiency} = \frac{\text{Weight of encapsulated drug in nanoparticles}}{\text{Weight of initial loading of drug}} \times 100\%$$

In vitro Drug Release Studies

The drug release characteristics of the arranged Fe_3O_4 @OA-CS-5-FLU-NP was determined as follows: 100 mg of the each Fe_3O_4@OA-CS-5-FLU-NP were placed in four individual glass beakers in 5 mL each containing phosphate buffer solutions of pH 7.4 and 5.2, respectively, along with 133 μM H_2O_2 placed on a mechanical shaker. Samples were collected (1 mL) at regular time intervals, and the concentration of 5-FLU released from the Fe_3O_4 @OA-CS-5-FLU-NP was determined by measuring the absorbance at 270 nm. The drug release efficiency of Fe_3O_4@OA-CS-5-FLU-NP was calculated using the following equation:

$$\text{Drug releasing efficiency}\,(\%) = \frac{C_t}{C_0 - C_t} \times 100$$

where C_t is the concentration of 5-FLU released from Fe_3O_4@OA-CS-5-FLU-NP at time "t" and C_0 is the initial concentration of the Fe_3O_4@OA-CS-5-FLU-NP.

In vitro Cytotoxicity Studies

MTT Cytotoxic Assay

A549, HeLa S3, MCF-7 and IMR-90 cells were purchased from ATCC, Manassas, VA, USA. A549, HeLa S3, MCF-7 and IMR-90 cell lines were cultured in DMEM medium (Dulbecco's Modified Eagle's Medium) and incubated at 37 ºC with 5% CO_2. Cells were seeded overnight onto 96-well plates at a density of 20,000 cells per well. After

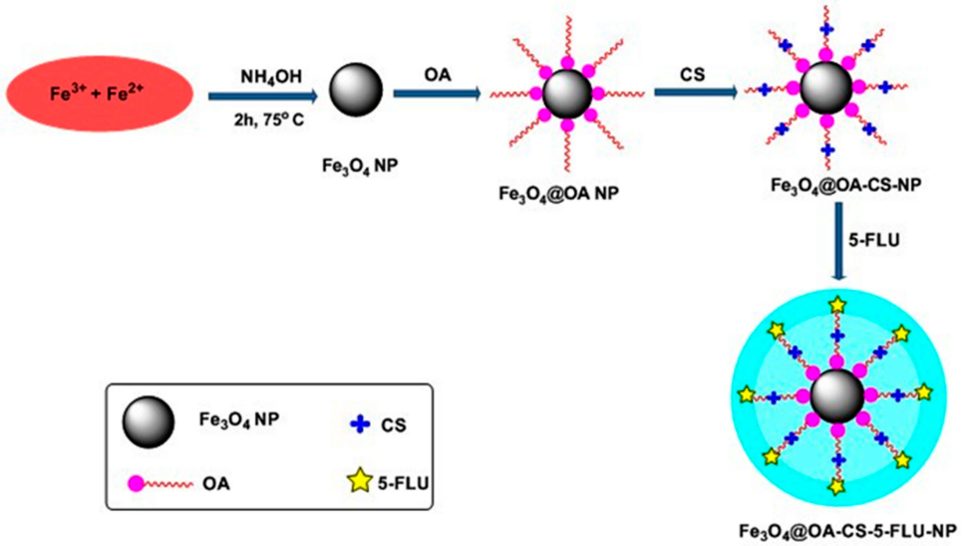

Figure 1 Schematic illustration of the preparation of Fe_3O_4@OA-CS-5-FLU-NP.

completion of the incubation period, the fresh medium containing blank nanoparticles or drug encapsulated nanoparticles were added to each well. Over a period of time, 10 µL of the (3-(4,5-dimethylthiazol-2-yl)-2,5-diphenyltetrazolium bromide) MTT solution (5 mg mL^{-1}) was added to each well, and then plates were further incubated for 4 h. Then, 100 µL of a formazan lysis solution (10% SDS in 0.1N HCl) was added to each well. The absorbance was measured at a wavelength of 570 nm using a microplate reader (BIO-RAD).

AO/EB Staining Assay

AO/EB fluorescence staining was performed to detect the morphological changes in apoptosis in A549 and HeLa S3 cells. Cells (1×10^5) maintained in DMEM for 24 h were exposed to 15 µg/mL (Fe_3O_4@OA-CS-5-FLU-NP) at 37 ºC and 5% CO_2. Then, 10 µL of a AO/EB dye was added to each well and further incubated for 15 min under dark conditions. The cells under fluorescence images were captured on a Biorevo, BZ-9000, Keyence (20x) fluorescence microscope system.

Colony Formation Assay

A549 and HeLa S3 (5×10^3 cells/well) cell lines were kept at 37°C in a humidified atmosphere containing 5% CO_2. Cells were cultured in DMEM medium and the A549 and HeLa S3 cells were washed twice with PBS buffer and incubated with various concentrations of MMS. After a period of time (10 days), the wells were washed with deionized water and stained with a crystal violet solution for 15 min. The obtained results were calculated by ImageJ software using colony area.

Statistical Analysis

Tests were completed at least three times each and the data were characterized as the average and standard deviation (mean ± SD) of three independent experiments. One-way ANOVA analysis was used for comparing between groups and $P < 0.05$ was considered a statistically significant difference.

Results and Discussion

Morphology and FTIR Analyses of Fe_3O_4@OA-CS-5-FLU-NPs

The surface morphology of the Fe_3O_4@OA-CS-5-FLU-NPs was analyzed through scanning electron micrographs (SEM). As depicted in Figure 2A, the nanoparticles appeared to be spherically-shaped with an average size of 1.5 µm and a smooth outer surface. Under an external magnetic field, Fe_3O_4@OA-CS-5-FLU-NP with a diameter of 50 nm can be selectively targeted to affected tissues.

The corresponding energy dispersive X-ray spectrum (EDX) of Fe_3O_4@OA-CS-5-FLU-NP is shown in Figure 2B. The characteristic peaks of carbon, nitrogen, oxygen and iron are presented by CS and 5-FLU. Furthermore, the metallic iron peaks show the existence of Fe_3O_4 NPs in the Fe_3O_4@OA-CS-5-FLU-NPs.

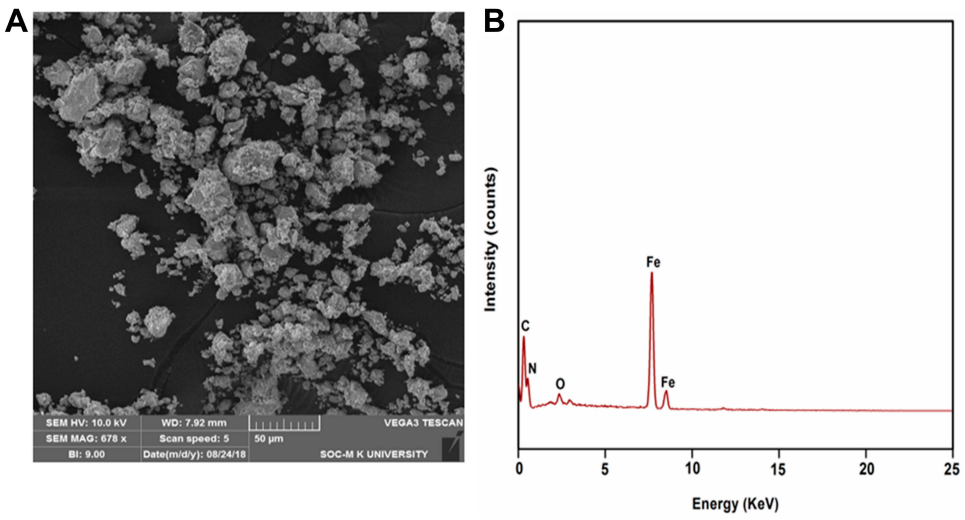

Figure 2 (**A**) SEM image and (**B**) EDX spectrum of Fe_3O_4@OA-CS-5-FLU-NP.

Due to the drying effects, aggregated SEM images for Fe_3O_4@OA-CS-5-FLU-NPs were achieved. EDX results clearly showed that CS and 5-FLU were loaded on the surface of the Fe_3O_4NPs. This is only supporting evidence. Meanwhile, the presence of CS and 5-FLU was further confirmed by FT-IR analysis (Figure 3). The FT-IR spectrum of Fe_3O_4 NPs showed a band at 580 cm^{-1} corresponding to Fe-O stretching. The characteristic O-H stretching of the hydroxyl group present in the oleic acid was observed at 3405 cm^{-1}. The peaks observed at 1395, 1612 and 2920 cm^{-1} corresponded to C-O, C=O and C-H stretching vibrations, respectively.[34] The FT-IR spectrum of CS showed a band at 3430 cm^{-1} for the O-H stretching vibration. Further, the peaks corresponding to 1660 cm^{-1} (C=O at amide I), 1660 cm^{-1} (N-H at amide II) and 885 cm^{-1} (C-N at amide III) correspond to –NH bending vibrations. 5-FLU

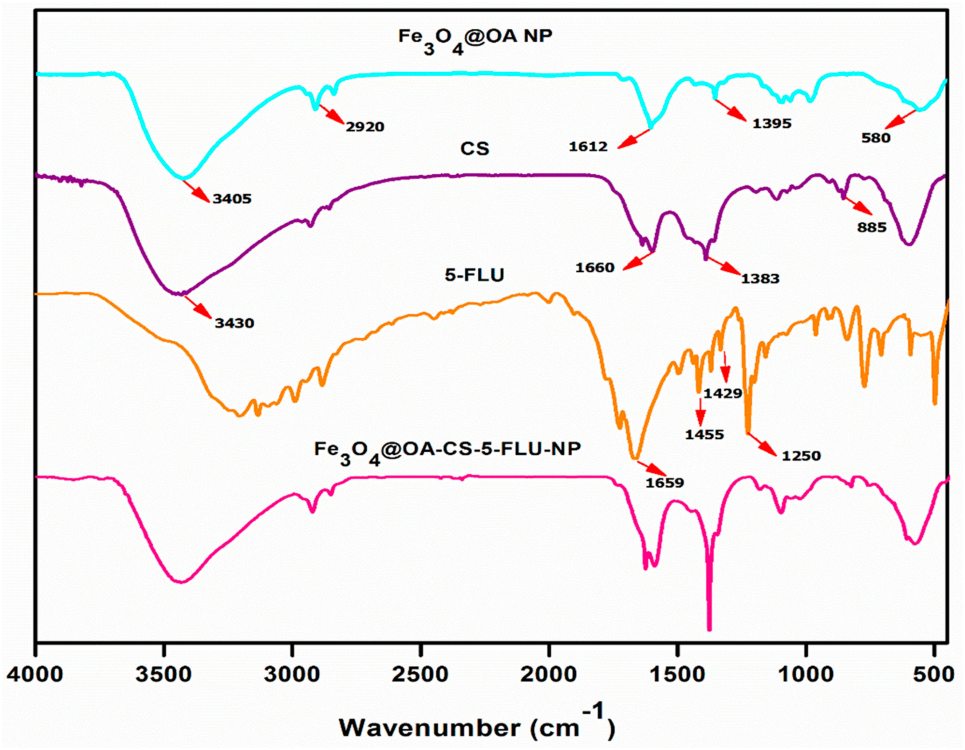

Figure 3 FT-IR spectrum of Fe_3O_4 NP, Fe_3O_4@OA NP, CS, 5-FLU and Fe_3O_4@ OA-CS-5-FLU-NP.

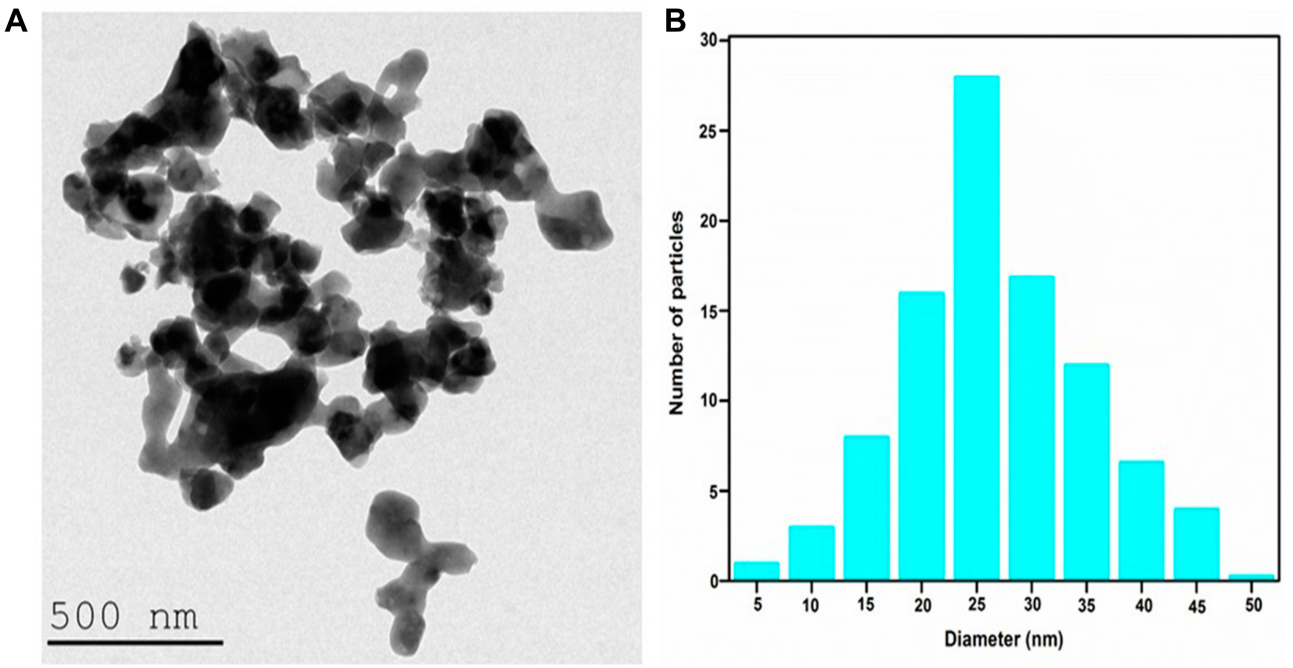

Figure 4 (**A**) TEM image and (**B**) Particle size distribution of Fe_3O_4@OA-CS-5-FLU-NP at 37 °C measured by dynamic light scattering.

displayed a broad vibrational band which appeared around 1659 cm^{-1} for the overlapping of peaks corresponding to the C=C, C=N, and C=O groups. The strong absorption bands observed at 1250 as well as 1429–1455 cm^{-1} can be assigned to the vibration of the multi-substituted pyrimidine compound and C-O, respectively. The FT-IR spectrum of Fe_3O_4@OA-CS-5-FLU-NP presented all the characteristic peaks of its components, such as Fe_3O_4@OA NP, CS, and 5-FLU and proved the successful formation of Fe_3O_4@ OA-CS-5-FLU-NP.[35]

Morphology and TEM Analyses of Fe_3O_4 @OA-CS-5-FLU-NPs

The morphology of the synthesized Fe_3O_4@OA-CS-5-FLU-NPs was characterized at 37°C using TEM analysis. The TEM image shown in Figure 4 for Fe_3O_4@OA-CS-5-FLU-NPs revealed that the magnetic nanoparticles agglomerated, and the average particle size was about 20–35 nm as measured by DLS. Thus, the polymer on the nanoparticles did not lead to aggregation between the particles.

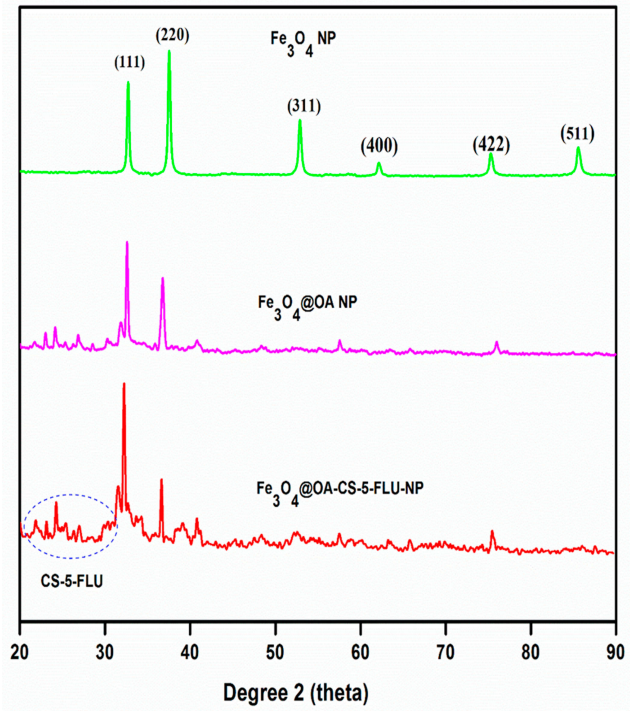

Figure 5 XRD patterns of Fe_3O_4 NP, Fe_3O_4@OA NP and Fe_3O_4@OA-CS-5-FLU-NP.

X-Ray Diffraction Analysis of Fe_3O_4 @OA-CS-5-FLU-NP

The crystalline nature of the Fe_3O_4NPs, Fe_3O_4@OA NPs and Fe_3O_4@OA-CS-5-FLU-NPs was analyzed by X-ray diffraction (Figure 5). Diffraction peaks were observed at 2θ values of 31.25°, 33.46°, 52.14°, 61.75°, 75.42° and 86.15° due to its crystalline nature. The Fe_3O_4@OA XRD pattern contained a slight semi-crystalline peak due to the surface attached oleate moiety. The respective peaks of the planes (311), (400), and

(511) were suppressed in Fe_3O_4@OA-CS-5-FLU due to the surface decorated OA, CS and 5-FLU. The crystalline nature of Fe_3O_4NP was retained even after loading of OA on the surface of the Fe_3O_4 NPs. It is suggested that the Fe_3O_4NPs in situ formed between the CS-5-FLU and the peak at the range of 2θ = 21.33–24.27° was assigned as the semi-crystalline response of CS-5-FLU.[36,37] The decoration of CS and 5-FLU on the surface of Fe_3O_4@OA NPs increased in intensity for the semi-crystalline peaks and this confirmed the successful formation of the Fe_3O_4@OA-CS-5-FLU-NPs.

Thermal Stability

TGA analysis of the Fe_3O_4@OA-CS-5-FLU-NPs was performed under inert conditions. Figure 6 shows the TGA curves of the Fe_3O_4@OA NPs and Fe_3O_4@OA-CS-5-FLU-NPs. The primary weight loss up to 100 °C might be the adsorbed water in those test mixtures. The TGA data showed the weight loss in the Fe_3O_4@OA NPs and a considerable decomposition was observed around 200–350 °C due to the loss of surface water. The obtained decomposition ~370–450°C matches the charged anticancer drug 5-FLU. The TGA of Fe_3O_4@OA had a weight loss curve in the range of 410–520 °C due to the decomposition of the coated OA.[38] These results indicated the reducing thermal strength of Fe_3O_4@OA NPs after the addition of the desired compositions of CS and 5-FLU in the Fe_3O_4@OA-CS-5-FLU-NPs.

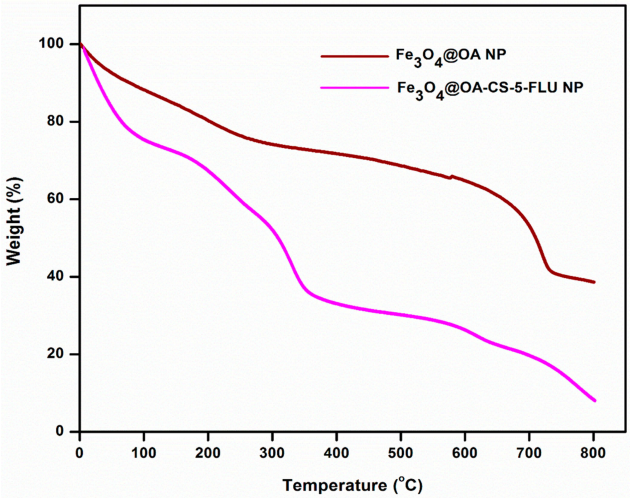

Figure 6 TGA curves of the Fe_3O_4@OA NP and Fe_3O_4@OA-CS-5-FLU-NP.

Magnetic Characteristic Analysis of Fe_3O_4@OA-CS-5-FLU-NPs

The magnetic properties of the Fe_3O_4@OA NPs and Fe_3O_4@OA-CS-5-FLU-NPs were studied by VSM at room temperature and the data is presented in Figure 7A. The higher saturation magnetization value of 73.25 emu/g was obtained

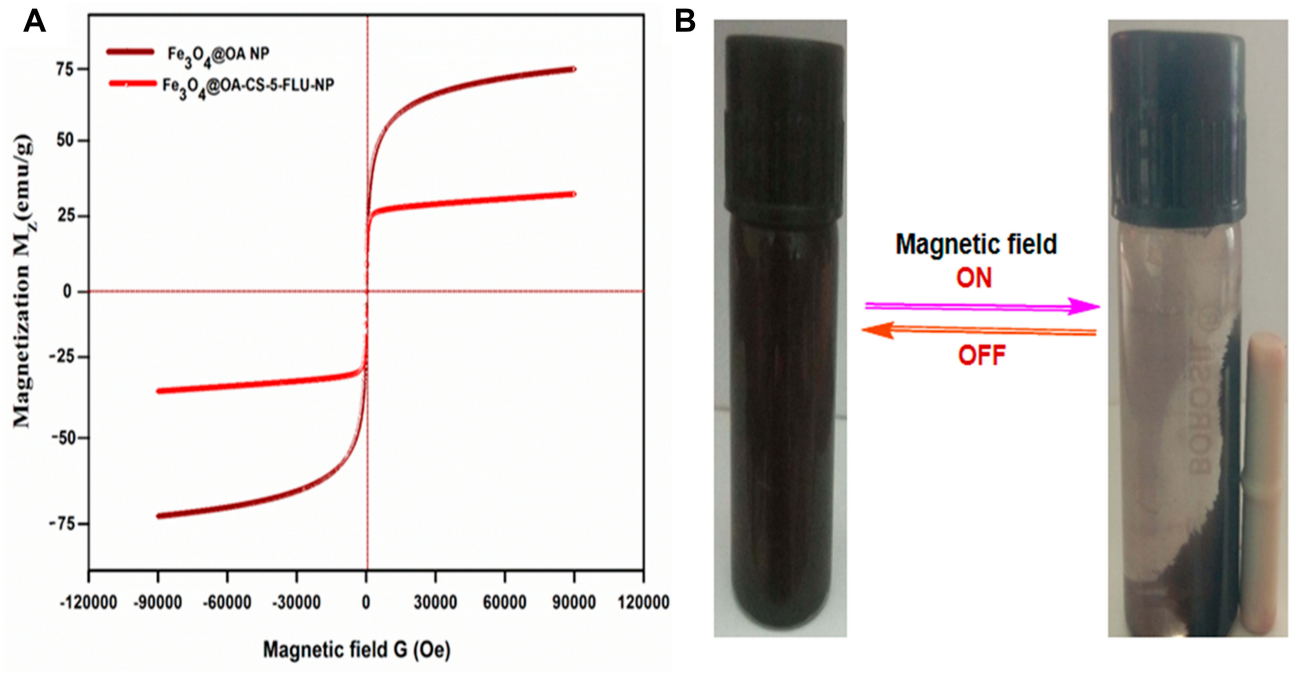

Figure 7 (**A**) Room temperature hysteresis curves of magnetite with Fe_3O_4@OA NP and Fe_3O_4@OA-CS-5-FLU-NP and (**B**) Magnetic field responsive behavior of Fe_3O_4@OA-CS-5-FLU-NP.

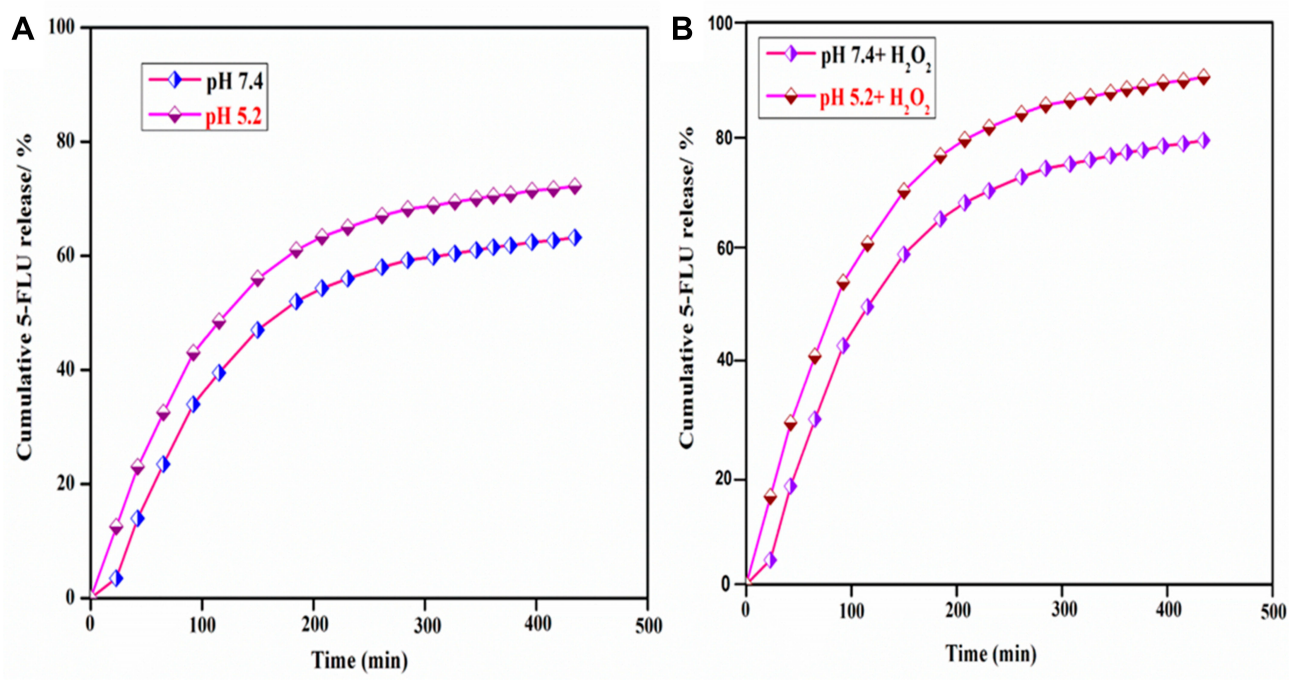

Figure 8 (**A**) Release curves at pH 7.4 and pH 5.2 in PBS containing Fe_3O_4@OA-CS-5-FLU-NPs. (**B**) 5-FLU release profile at pH 7.4 (H_2O_2) and pH 5.2 (H_2O_2) in PBS containing Fe_3O_4@OA-CS-5-FLU-NP.

for the Fe_3O_4@OA NPs. However, a lower saturation magnetization of 30.21 emu/g was found for the Fe_3O_4@OA-CS -5-FLU-NPs. Hence, the gained magnetic targeted drug-delivery for these NPs has potential for broad biomedical applications. The lower value of the saturation magnetization is due to the smaller size of the nanoparticles and the low saturation magnetization of the Fe_3O_4@OA-CS-5-FLU-NP composite may be attributed to the presence of a thick polymeric layer of CS and 5-FLU on the Fe_3O_4@OA NPs.[39] The Fe_3O_4@OA-CS-5-FLU-NPs also retained superior paramagnetic properties at room temperature which is useful in a drug-releasing system. As they do not retain magnetization before and after exposure to an external localized magnetic field, this reduces the probability of particle aggregation due to magnetic dipole attraction. The higher magnetization of the Fe_3O_4@OA-CS-5-FLU-NPs is useful for magnetically targeted drug-delivery systems. Hence, the magnetic performances of Fe_3O_4@OA-CS-5-FLU-NPs (Figure 7B) afford good targeted ability for therapeutic applications.

In vitro Drug Release Studies

Accordingly, these nanoparticles might exhibit cytotoxic activity as carrier molecules consisting of OA along with the drug which could be absorbed by simple diffusion. The in vitro release of 5-FLU from the Fe_3O_4@OA-CS-5-FLU-NP aggregates was studied in PBS at different pH values as illustrated in Figure 8A. At the physiological pH of 7.4, 5-FLU uptake (as determined was adsorbed on the Fe_3O_4 @OA-CS-5-FLU-NPs) was released very slowly and the amount of the released 5-FLU presented as a weight

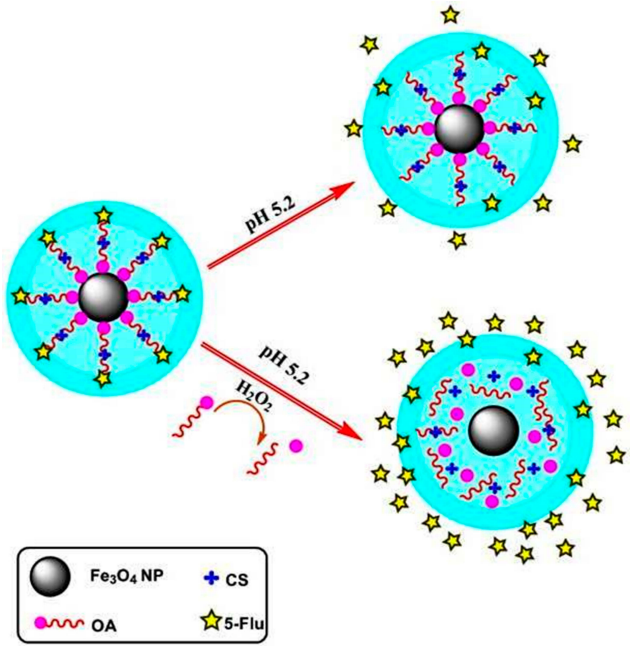

Figure 9 Schematic representation of ROS activated 5-FLU release from Fe_3O_4 @OA-CS-5-FLU-NP in a cancerous cell mimicking pH (5.2) medium.

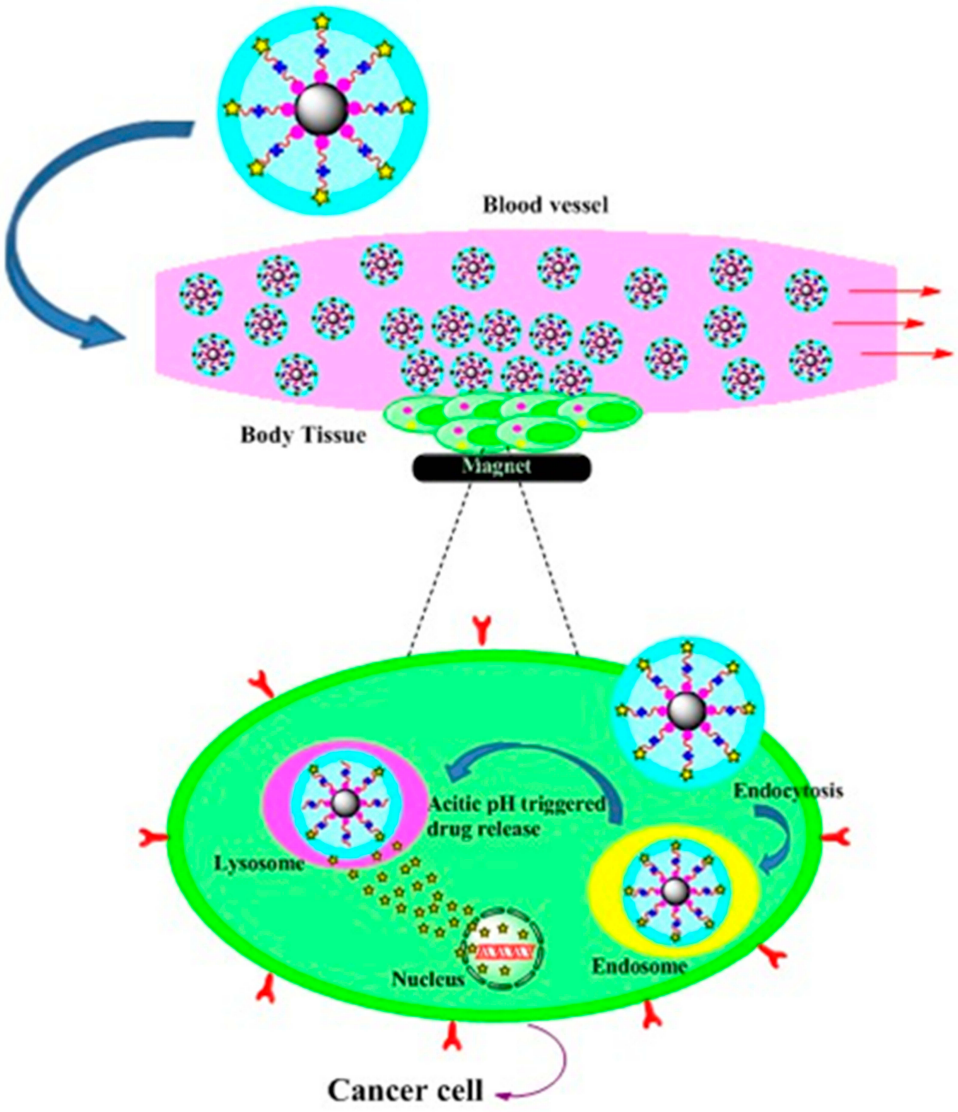

Figure 10 Schematic illustration showing the magnetically targeted pH 5.2 (H_2O_2) in PBS as a responsive 5-FLU release process from the Fe_3O_4@OA-CS-5-FLU-NP.

percentage of the total 5-FLU adsorbed, was only about 62% over a period of 500 min. In contrast, in PBS at pH 5.2, to mimic the intracellular conditions of cancer cells, the release rate of 5-FLU from the Fe_3O_4@OA-CS-5-FLU-NP was much faster and the highest release of 5-FLU was over 73% within 500 min.[40] Furthermore, in acidic conditions, the 5-FLU released in a biologically active manner and as an anti-metabolite of the pyrimidine analogue. In acidic medium (pH 5.2), -NH_2 groups in the CS polymer matrix stayed simply protonated into –NH_3^+groups, which can weaken hydrogen bonding interactions between the CS polymer which was dissolved in a buffer solution, and released over the diffusion process.[41] It is well known that chitosan is soluble in water in acidic media (pH = 2–6). At this pH, chitosan swells and its chains undergo deployment due to the electrostatic repulsion of positively charged –NH^{3+} groups. These results indicated that the release of 5-FLU from the NPs can be measured by changing the pH, which may facilitate its drug delivery and controlled discharge into cancer cells since the microenvironment of the extracellular tissues of tumors and intracellular lysosomes and endosomes are acidic.[42–44]

In additional analysis, for the site-specific drug delivery of Fe_3O_4@OA-CS-5-FLU-NP in cancer, the 5-FLU release behavior from Fe_3O_4@OA-CS-5-FLU-NPs was carried out at pH 5.2 in the presence of H_2O_2. The 5-FLU release rate from Fe_3O_4@OA-CS-5-FLU-NP at pH 7.4 was very low, while at pH 5.2, there was a high

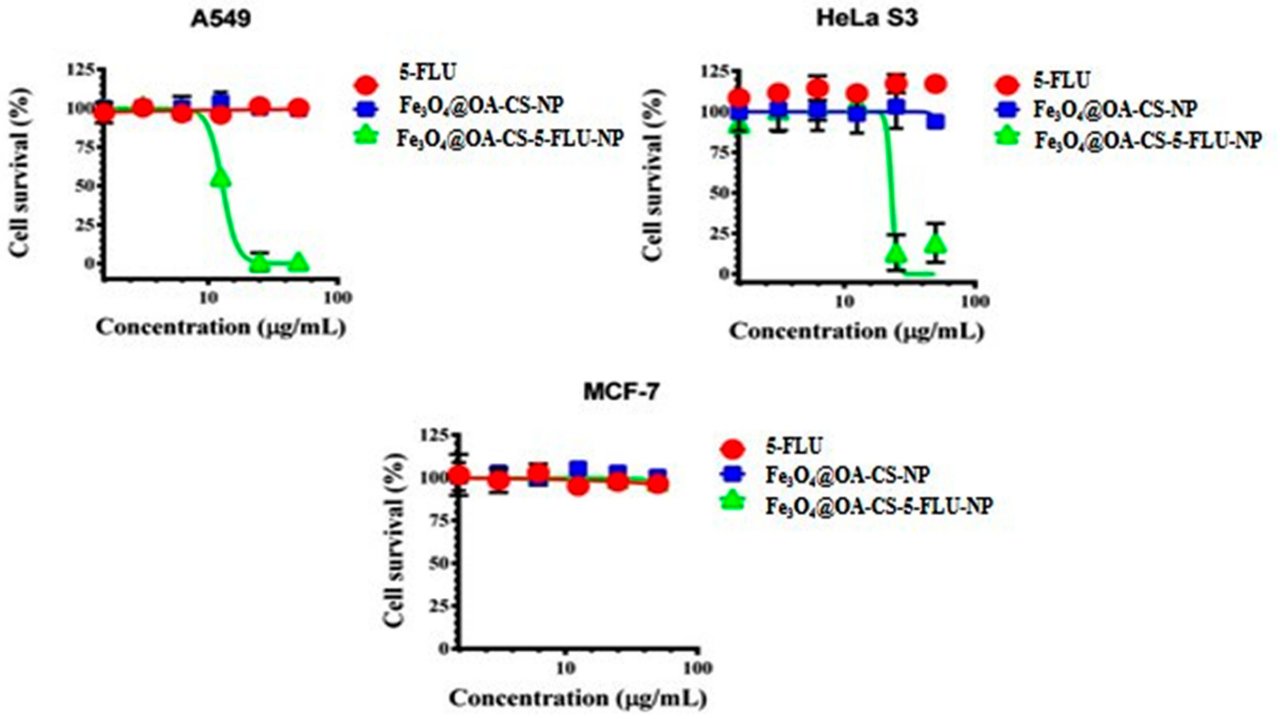

Figure 11 Cytotoxic studies of nanoparticles examined by MTT assays against human A549, Hela S3 and MCF-7 cancer cells. The experiments were conducted three times and the data expressed as mean ± SD of individual and statistical data were analyzed using GraphPad Prism 6 software.

rate of 5-FLU released in a controlled fashion, simplifying the release of 5-FLU in carcinogenic cells as biologically active. The experimental results exposed that the pH-dependent 5-FLU release from the Fe_3O_4@OA-CS -5-FLU-NPs also led to a high releasing proficiency in the presence of ROS (H_2O_2). The rate of 5-FLU release in the presence of H_2O_2 was higher than in the absence of H_2O_2 at pH 5.2; almost 90% of the 5-FLU was released after 450 min (Figure 8B), although only 70% of the 5-FLU was released at pH 5.2 in the absence of H_2O_2.

It is assumed that only the CS layer degraded at pH 5.2 which led to the release of 5-FLU, but in the presence of H_2O_2, the OA layer also degraded (at the same time breaking of bonds amongst the hydrophilic as well as hydrophobic part of OA) which facilitated a high release of 5-FLU from the Fe_3O_4@OA-CS-5-FLU-NPs; OA acts as a modifier in nanoparticle synthesis. OA showed good dispersion ability, and which could be ascribed to the great reduction in high surface energy and dipolar attraction of the nanoparticles.[45] These results clearly exposed that the Fe_3O_4@OA-CS -5-FLU-NP had favorable 5-FLU release in the presence of ROS (Figure 9), and that the Fe_3O_4@OA-CS-5-FLU-NP are suitable carriers to deliver 5-FLU at targeted cancerous cell sites without worrying about primary release in the circulation.[46] Also, the 5-FLU releasing efficiency from the Fe_3O_4@OA-CS-5-FLU-NPs increased with an increase of the mixed concentrations of CS. The increase in polymer concentration led to an increase in both particle size and encapsulation efficiency of the prepared NPs. This was attributed to the increased viscosity that helped to enlarge the size and maximize encapsulation efficiency.[47]

Table 1 IC50 Values of the Synthesized NPs Against Human A549, HeLa S3, MCF-7 and IMR-90 Cells

Complex	A549 (µg/mL)	HeLa S3 (µg/mL)	MCF-7 (µg/mL)	IMR-90 (µg/mL)
5-FLU	>50	>50	>50	NT
Fe_3O_4@OA-CS-NP	>50	>50	>50	NT
Fe_3O_4@OA-CS-5-FLU-NP	12.9	23	>50	>50

Abbreviation: NT, not tested.

The 5-FLU release from the Fe_3O_4@OA-CS-5-FLU-NP at pH 5.2 (H_2O_2 in PBS) demonstrated a high amount of 5-FLU released in a controlled manner, as shown in Figure 10. The release of 5-FLU in cancerous cells was also biologically active under acidic conditions. Due to its

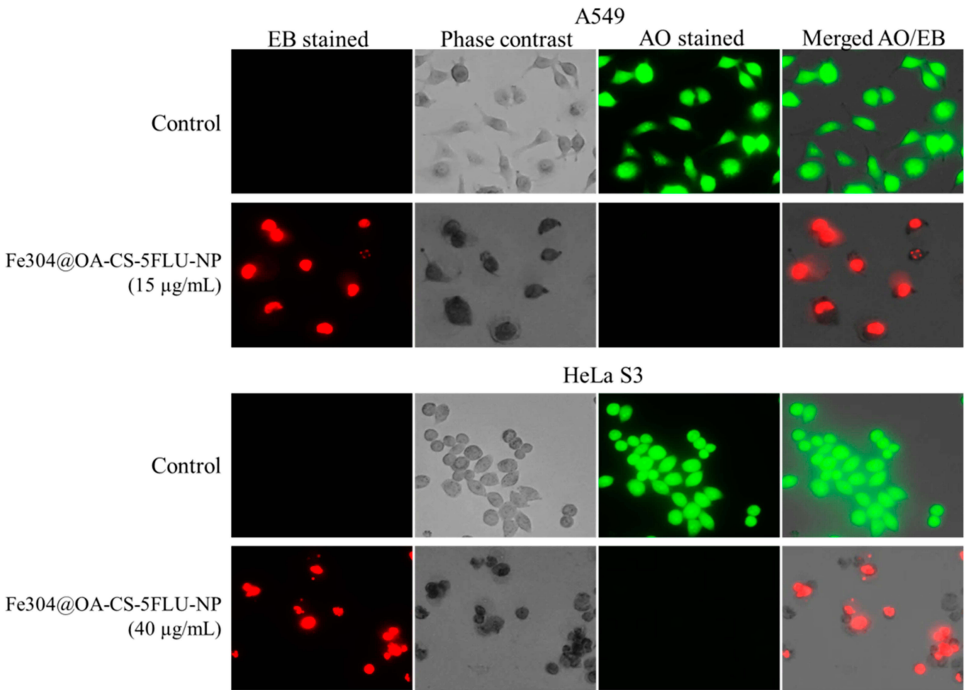

Figure 12 Mode of cell death as analyzed by fluorescence microscopy (Biorevo, BZ-9000, Keyence) using EB and AO after the addition of active Fe_3O_4@OA-CS-5-FLU-NP in A549 and HeLa S3 cells. Red color indicates dead cells and green color indicates live cells tested with 15 and 40 µg/mL for 24 h at 37°C. Scale bar: 50 µm.

structure, 5-FLU hinders nucleoside metabolism and can be combined into RNA and DNA, leading to cytotoxicity and cell death. Moreover, powerful scavengers of free-radical oxidants result via H-atom donation as well as electron transfer, exerting their antioxidant activity.[48–50] However, the Fe_3O_4@OA-CS-5-FLU-NPs exhibited 5-FLU release at pH 5.2, indicating the nature of the loaded 5-FLU suggesting that the Fe_3O_4@OA-CS-5-FLU-NPs are proper carriers to deliver 5-FLU to targeted cancerous cell sites without early release.

In vitro Anticancer Studies

To further investigate the cell-toxic properties of the nanoparticles, including 5-FLU and Fe_3O_4@OA-CS-NPs and Fe_3O_4@OA-CS-5-FLU-NPs, to A549, HeLa S3 and MCF-7 cells, MTT assays using different concentrations (1.5–50 µg/mL) for 24 h at 37º C were conducted. As depicted in Figure 11 and Table 1, the viability of the A549, HeLa S3 and MCF-7 cells in the presence of Fe_3O_4 @OA-CS-5-FLU-NPs displayed higher cytotoxicity against A549 and HeLa S3 cells with IC50 values after 24 h of 12.9 and 23 µg/mL, respectively. In addition, A549, HeLa S3 and MCF-7 cell viability did not change by Fe_3O_4@OA-CS-NP exposure. Further, toxicity studies on 5-FLU and Fe_3O_4 @OA-CS-5-FLU-NP for human normal lung IMR-90 cells were conducted by MTT assays. Remarkably, both 5-FLU and Fe_3O_4@OA-CS-5-FLU-NPs, did not show toxicity up to >50 µg/mL for IMR-90 cells.[51] The Fe_3O_4 nanoparticle aggregates of different sizes were characterized for their uptake and toxicity in three different cell lines. While the aggregation did not elicit a unique toxic response, the uptake patterns were different between single and aggregated nanoparticles. There was a decrease in uptake of aggregated nanoparticles by HeLa S3 and A549 cells in comparison to single and monodispersed nanoparticles.

In addition, the cytotoxic study revealed cell morphological modifications and nucleus fragmentation using a co-staining process with acridine orange (AO) and ethidium bromide (EB) of A549 and HeLa S3 cells. Here, AO was used as a staining reagent of live cells and EB was used as an indicator for dead cells. A549 and HeLa S3 cells were examined in the presence of Fe_3O_4@OA-CS-5-FLU-NPs (15 and 40 µg/mL) for 24 h and pictures were captured with the help of AO/EB under fluorescence microscopy. As presented in Figure 12, in the presence of Fe_3O_4@OA-CS-5-FLU-NPs, cell death of A549 and HeLa S3 cells gradually increased as specified by the red color which co-stained EB.[52]

Moreover, this study further investigated whether the Fe_3O_4@OA-CS-5-FLU-NPs had an ability to control A549 and HeLa S3 cell colonization. As shown in Figure 13, complete inhibition of colony development was demonstrated in the presence of Fe_3O_4@OA-CS-5-FLU-NPs

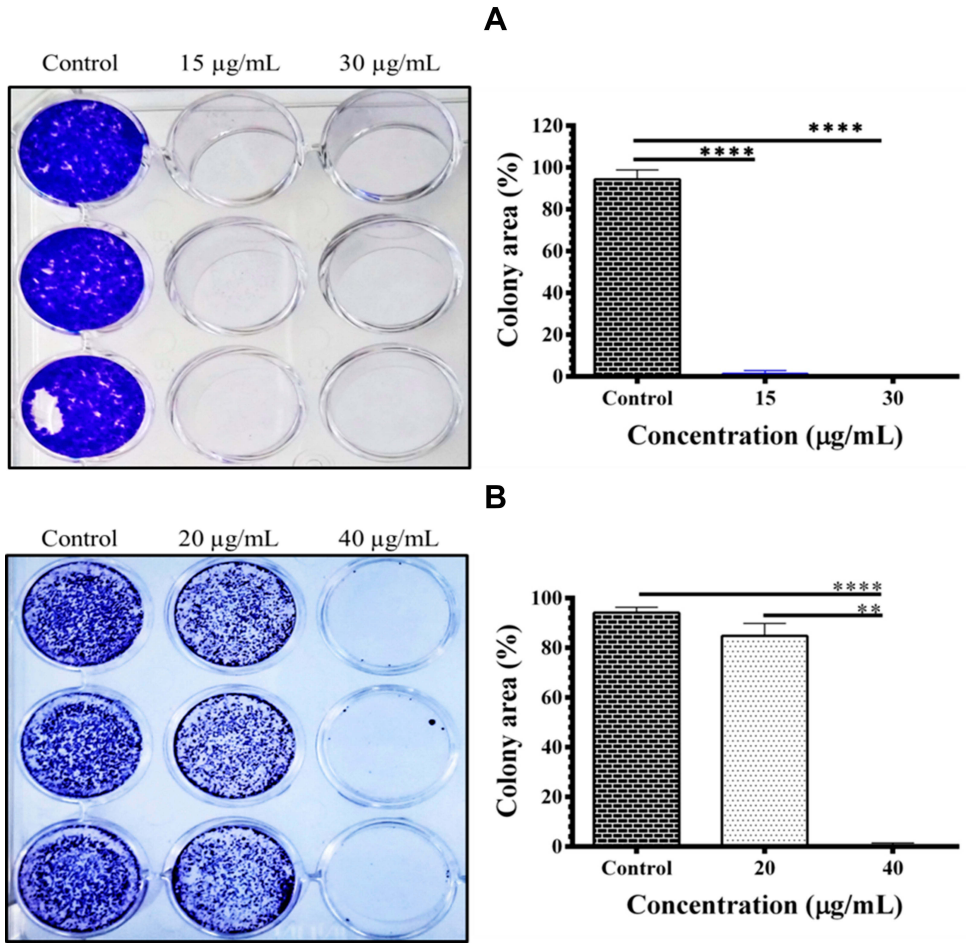

Figure 13 Colony formation in the presence of Fe_3O_4@OA-CS-5-FLU-NP examined against A549 and HeLa S3 cells: (**A**) A549 and (**B**) HeLa S3 cells. The colony area was calculated by ImageJ software using colony area (mean ± SD). Significance of ****$p < 0.0001$ and **$p<0.01$ as compared with the untreated control group.

against A549 and HeLa S3 cells at 15 and 40µg/mL, respectively. However, Fe_3O_4@OA-CS-5-FLU-NPs did not affect cell colony formation at a lower concentration of 20µg/mL for the Hela S3 cells. Finally, we conclude here that the Fe_3O_4@OA-CS-5-FLU-NPs not only showed cytotoxicity (including morphological changes) but also showed a capability to reduce the colony formation of A549 and HeLa S3 cells.[53]

Conclusion

In summary, Fe_3O_4@OA-CS-5-FLU-NPs were synthesized by an easy and quick in situ loading method. The proposed Fe_3O_4@OA-CS-5-FLU-NPs were successfully prepared as well as characterized by several spectroscopic and microscopic studies. They showed significant ROS reactive drug-releasing properties. Further, the Fe_3O_4@OA-CS-5-FLU-NPs showed promising magnetic properties that could be used for magnetic targeted and pH-responsive drug-delivery systems. The pH triggered drug release of 5-FLU from Fe_3O_4@OA-CS-5-FLU-NPs includes the ROS-responsive polymeric nanocarriers under marginally acidic conditions of pH 5.2 and pH of 7.4. Meanwhile, the MTT assay, fluorescence staining as well as colony formation assay results, revealed that the Fe_3O_4@OA-CS-5-FLU-NPs are active and safe for anticancer biomedical applications, and thus should be further studied.

Acknowledgments

The authors are thankful to the Department of Science and Technology and Science and Engineering Research Board (DST-SERB, Grant No. SB/FT/CS-130/2012, the Government of India, New Delhi) for funding this work. The authors greatly acknowledge the Chikkanna Government Arts College, Tirupur and the Mohamed Sathak Engineering College, Kilakkarai for providing lab and instrumentation facilities.

Disclosure

The authors have no conflicts of interest to declare.

References

1. Wong HL, Bendayan R, Rauth AM, Li Y, Wu XY. Chemotherapy with anticancer drugs encapsulated in solid lipid nanoparticles. *Advan Drug Deliv Rev*. 2007;59(6):491–504. doi:10.1016/j.addr.2007.04.008
2. Durán JDG, Arias JL, Gallardo V, Delgado AV. Magnetic colloids as drug vehicles. *J Pharm Sci*. 2008;97(8):2948–2983. doi:10.1002/jps.21249
3. Zhang N, Yin Y, Xu SJ, Chen WS. 5-fluorouracil: mechanisms of resistance and reversal strategies. *Molecules*. 2008;13(8):1551–1569. doi:10.3390/molecules13081551
4. Arias JL, Ruiz MA, López-Viota M, Delgado AV. Poly(alkylcyanoacrylate) colloidal particles as vehicles for antitumour drug delivery: a comparative study. *Colloids Surf B Biointerfaces*. 2008;62(1):64–70. doi:10.1016/j.colsurfb.2007.09.018
5. Zhu K, Ye T, Liu J, et al. Nanogels fabricated by lysozyme and sodium carboxymethyl cellulose for 5-fluorouracil controlled release. *Int J Pharm*. 2013;441(1–2):721–727. doi:10.1016/j.ijpharm.2012.10.022.
6. Qi D, Lu J, Deng C, Zhang XJ. Magnetically responsive Fe3O4@C@SnO 2 core–shell microspheres: synthesis, characterization and application in phosphoproteomics. *Phys Chem C*. 2009;113(36):15854–15861. doi:10.1021/jp902959d
7. Liu Y, Wang Y, Zhou S, et al. Controllable synthesis of hierarchical porous Fe_3O_4 particles mediated by poly(diallyldimethylammonium chloride) and their application in arsenic removal. *ACS Appl Mater Interfaces*. 2013;5(23):12449–12459.
8. Spanakis M, Bouropoulos N, Theodoropoulos D, Sygellou L, Ewart S, Moschovi AM. Inclusion of new 5-fluorouracil amphiphilic derivatives in liposome formulation for cancer treatment. *J Med Chem Commun*. 2015;6(9):1639–1642.
9. Mornet S, Portier J, Duguet E. A method for synthesis and functionalization of ultrasmall superparamagnetic covalent carriers based on maghemite and dextran. *J Magn Magn Mater*. 2005;293(1):127–134. doi:10.1016/j.jmmm.2005.01.053
10. Spanova A, Horak D, Soudkova E, Rittich B. Magnetic hydrophilic methacrylate-based polymer microspheres designed for polymerase chain reactions applications. *J Chromatogr B*. 2004;800(1–2):27–32. doi:10.1016/j.jchromb.2003.09.010
11. Omi S, Kanetaka A, Shimamori Y, Supsakulchai A, Nagai M, Ma GH. Magnetite (Fe_3O_4) microcapsules prepared using a glass membrane and solvent removal. *J Microencapsul*. 2001;18(6):749–765.
12. Caruso F, Susha AS, Giersig M, Mohwald H. Magnetic core-shell particles preparation of magnetite multilayers on polymer latex microspheres. *Adv Mater*. 1999;11(11):950–953. doi:10.1002/(SICI)1521-4095(199908)11:11<950::AID-ADMA950>3.0.CO;2-T
13. Liu ZM, Liu YL, Yang HF, Yang Y, Shen GL, Yu RQ. A phenol biosensor based on immobilizing tyrosinase to modified core-shell magnetic nanoparticles supported at a carbon paste electrode. *Anal Chim Acta*. 2005;533(11):3–9.
14. Chatterjee J, Haik Y, Chen CJ. Synthesis and characterization of heat-stabilized albumin magnetic microspheres. *Colloid Polym Sci*. 2001;279(11):1073–1081. doi:10.1007/s003960100523
15. Levy L, Sahoo Y, Kim KS, Bergey EJ, Prasad PN. Nanochemistry: synthesis and characterization of multifunctional nanoclinics for biological applications. *Chem Mater*. 2002;14(9):3715–3721. doi:10.1021/cm0203013
16. Shahani K, Panyam J. Highly loaded sustained-release microparticles of curcumin for chemoprevention. *J Pharm Sci*. 2011;100(7):2599–2609. doi:10.1002/jps.22475
17. Gupta AK, Gupta M. Synthesis and surface engineering of iron oxide nanoparticles for biomedical applications. *Biomaterials*. 2005;26(18):3995–4021. doi:10.1016/j.biomaterials.2004.10.012
18. Zhang XY, Wang LXJ. Effects of surface modification on the properties of magnetic nanoparticles/PLA composite drug carriers and in vitro controlled release study. *Colloid Surf A-Physicochem Eng*. 2013;431(2013):80–86. doi:10.1016/j.colsurfa.2013.04.021
19. Zhang XY, Wang LXJ, Wang J. Development and characterization of size controlled polymeric microcapsules loaded with super paramagnetic nanoparticles. *Polym Compos*. 2013;34(4):443–449. doi:10.1002/pc.22429
20. Unsoy G, Yalcin S, Khodadust R, Gunduz G, Gunduz U. Synthesis optimization and characterization of chitosan coated iron oxide nanoparticles produced for biomedical applications. *J Nanopart Res*. 2012;14(11):1–13.
21. Li FX, Li XI, Li B. Preparation of magnetic polylactic acid microspheres and investigation of its releasing property for loading curcumin. *J Magn Magn Mater*. 2011;323(22):2770–2775. doi:10.1016/j.jmmm.2011.05.045
22. Wei ZJ, Wang CY, Liu H, Zou SW, Tong Z. Systematic studies of pickering emulsions stabilized by uniform-sized PLGA particles: preparation and stabilization mechanism. *Colloids Surf B*. 2012;91(2012):97–105. doi:10.1016/j.colsurfb.2011.10.044
23. Liu X, Kaminski MD, Chen H, Torno M, Taylor LA, Rosengart J. Synthesis and characterization of highly-magnetic biodegradable poly (d,l-lactide-co-glycolide) nanospheres. *J Control Release*. 2007;119(1):52–58. doi:10.1016/j.jconrel.2006.11.031
24. Xu A, Dou HJ, Shi WB, et al. "Two-in-one" fabrication of Fe3O4/MePEG-PLA composite nanocapsules as a potential ultrasonic/MRI dual contrast agent. *Langmuir*. 2011;27(19):12134–12142. doi:10.1021/la202096x
25. Mu B, Zhong W, Dong Y, Du PC, Liu P. Encapsulation of drug microparticles with self-assembled Fe_3O_4/alginate hybrid multilayers for targeted controlled release. *J Biomed Mater Res B*. 2012;100B(3):825–831. doi:10.1002/jbm.b.32646
26. Arias JL, Ruiz M, Gallardo V, Delgado AV. Tegafur loading and release properties of magnetite/poly (alkylcyanoacrylate) (core/shell) nanoparticles. *J Control Release*. 2008;125(1):50–58. doi:10.1016/j.jconrel.2007.09.008
27. Zhou L, He B, Zhang F. Facile one-pot synthesis of iron oxide nanoparticles cross-linked magnetic poly(vinyl alcohol) gel beads for drug delivery. *ACS Appl Mater Interfaces*. 2012;4(1):192–199. doi:10.1021/am201649b
28. Khosroshahi ME, Ghazanfari L. Preparation and rheological studies of uncoated and PVA-coated magnetite nanofluid. *J Magn Magn Mater*. 2012;324(24):4143–4146. doi:10.1016/j.jmmm.2012.07.025
29. McConville P, Pope JM. A comparison of water binding and mobility in contact lens hydrogels from NMR measurements of the water self-diffusion coefficient. *Polymer*. 2000;41(26):9081–9088. doi:10.1016/S0032-3861(00)00295-0
30. Latorre A, Couleaud P, Aires A, Cortajarena AL, Somoza Á. Multifunctionalization of magnetic nanoparticles for controlled drug release: a general approach. *Eur J Med Chem*. 2014;82(2014):355–362. doi:10.1016/j.ejmech.2014.05.078
31. Pham XN, Nguyen TP, Pham TN, Tran TTN, Tran TVT. Synthesis and characterization of chitosan-coated magnetite nanoparticles and their application in curcumin drug delivery. *Adv Nat Sci-Nanosci Nanotech*. 2016;7(4):045010. doi:10.1088/2043-6262/7/4/045010
32. Dilnawaz F, Singh A, Mohanty C, Sahoo SK. Dual drug loaded superparamagnetic iron oxide nanoparticles for targeted cancer therapy. *Biomaterials*. 2010;31(13):3694–3706. doi:10.1016/j.biomaterials.2010.01.057
33. Bani D, Bencini A, Bergonzi MC, et al. Enhanced intra-cutaneous delivery of a Mn-containing antioxidant drug by high frequency ultrasounds. *J Pharmaceut Biomed Anal*. 2015;106(2015):197–203. doi:10.1016/j.jpba.2014.11.021

34. Li P, Wanga Y, Pengb Z, Shea F, Konga L. Development of chitosan nanoparticles as drug delivery systems for 5-fluorouracil and leucovorin blends. *Carbohydr Polym*. 2011;85(3):698–704. doi:10.1016/j.carbpol.2011.03.045
35. Zhang LY, Zhu XJ, Sun HW, Chi GR, Xu JX, Sun YI. Control synthesis of magnetic Fe3O4–chitosan nanoparticles under UV irradiation in aqueous system. *Curr Appl Phys*. 2010;10(3):828–833. doi:10.1016/j.cap.2009.10.002
36. Sekhar EC, Rao KK, Raju, RR. Chitosan/guargum-g-acrylamide semi IPN microspheres for controlled release studies of 5-Fluorouracil. *J Appl Pharm Sci*. 2011;1(8):199–204.
37. Nivethaa EAK, Dhanavel S, Narayanan V, Vasu CA, Stephen, A. An in vitro cytotoxicity study of 5-fluorouracil encapsulated chitosan/gold nanocomposites towards MCF-7 cells. *RSC Adv*. 2015;5(2):1024–1032. doi:10.1039/C4RA11615A
38. Bhatt AS, Bhat DK, Santosh MS. Electrical and magnetic properties of chitosan-magnetite nanocomposites. *Physica B Condens Matter*. 2010;405(8):2078–2082. doi:10.1016/j.physb.2010.01.106
39. Liu J, Che R, Chen H. Microwave absorption enhancement of multifunctional composite microspheres with spinel Fe_3O_4cores and anatase TiO_2shells. *Small*. 2012;8(8):1214–1221. doi:10.1002/smll.201102245
40. Samad AA, Bakkour Y, Fanny C, Omar FE, Coudane J, Nottelet B. From nanospheres to micelles: simple control of PCL-g-PEG copolymers' amphiphilicity through thiol–ynephotografting. *Polym Chem*. 2015;6(28):5093–5102. doi:10.1039/C5PY00391A
41. Pylypchuk IV, Kołodyńska D, Kozioł M, Gorbyk PP. Gd-DTPA adsorption on chitosan/magnetite nanocomposites. *Nanoscale Res Lett*. 2016;11(1):168. doi:10.1186/s11671-016-1363-3
42. Chopra D, Ray L, Dwivedi A, et al. Photoprotective efficiency of PLGA-curcumin nanoparticles versus curcumin through the involvement of ERK/AKT pathway under ambient UV-R exposure in HaCaT cell line. *Biomaterials*. 2016;84(2016):25–41. doi:10.1016/j.biomaterials.2016.01.018
43. Chen H, Zhang W, Zhu G, Xie J, Chen X. Rethinking cancer nanotheranostics. *Nat Rev Mater*. 2017;2(7):17024. doi:10.1038/natrevmats.2017.24
44. Jo SD, Ku SH, Won YY, Kim SH, Kwon IC. Targeted nanotheranostics for future personalized medicine: recent progress in cancer therapy. *Theranostics*. 2016;6(9):1362–1377. doi:10.7150/thno.15335
45. Ayyanaar S, Kesavan MP, Palpandi Raja R, Rajagopal G, Rajagopal G, Rajagopal G. Reactive oxygen species (ROS)-responsive microspheres for targeted drug delivery of camptothecin. *J Drug Deliv Sci Tec*. 2019;52(2019):722–729. doi:10.1016/j.jddst.2019.05.036
46. Muthu MS, Leong DT, Mei L, Feng SS. Nanotheranostics-application and further development of nanomedicine strategies for advanced theranostics. *Theranostics*. 2014;4(6):660–677. doi:10.7150/thno.8698
47. Aldawsari HM. Fluconazole nano-particles loaded gel for improved efficacy in treatment of oral candidiasis. *Pharmacology*. 2019;15(3):436–440.
48. Dharmaraja AT. Role of reactive oxygen species (ROS) in therapeutics and drug resistance in cancer and bacteria. *J Med Chem*. 2017;60(8):3221–3240. doi:10.1021/acs.jmedchem.6b01243
49. Jeschek D, Lhota G, Wallner J, Vorauer-Uhl K. A versatile, quantitative analytical method for pharmaceutical relevant lipids in drug delivery systems. *J Pharmaceut Biomed Anal*. 2016;11:37–44.
50. Peng Z, Yang X, Qin J. Glyoxalase-1 overexpression reverses defective proangiogenic function of diabetic adipose-derived stem cells in streptozotocin-induced diabetic mice model of critical limb ischemia. *Stem Cells Transl Med*. 2017;6(1):261–271. doi:10.5966/sctm.2015-0380
51. Denu RA, Hematti P. Effects of oxidative stress on mesenchymal stem cell biology. *Oxid Med Cell Longev*. 2016;2016:2989076.
52. Sun Y, Hu X, Hu G, Xu C, Jiang H. Curcumin attenuates hydrogen peroxide-induced premature senescence via the activation of SIRT1 in human umbilical vein endothelial cells. *Biol Pharm Bull*. 2015;38(8):1134–1141. doi:10.1248/bpb.b15-00012
53. Kukongviriyapan U, Apaijit K, Kukongviriyapan V. Oxidative stress and cardiovascular dysfunction associated with cadmium exposure: beneficial effects of curcumin and tetrahydrocurcumin. *Tohoku J Exp Med*. 2016;239(1):25–38. doi:10.1620/tjem.239.25